Turbulent drag reduction by anisotropic permeable coatings

G. Gomez-de-Segura, A. Sharma, R. Garcia-Mayoral

Department of Engineering
University of Cambridge
Trumpington St, Cambridge CB2 1PZ, UK
gg406@cam.ac.uk, as2527@cam.ac.uk, r.gmayoral@eng.cam.ac.uk

ABSTRACT

The behaviour of turbulent flow over anisotropic permeable substrates is analysed numerically through linear stability analysis and Direct Numerical Simulation (DNS). The flow within the permeable substrate is modelled by the Brinkman equation, which is solved analytically to obtain the boundary conditions at the substrate-channel interface for both the DNS and stability analysis. The linear stability analysis is used as an a priori model to capture the onset of drag-increasing Kelvin-Helmholtz rollers. The associated instability is essentially driven by the wall-normal permeability K_y^+. DNS corroborates that the drag decreasing effect of slip is offset by the drag increasing effect of the wall-normal transpiration. The latter is associated with the presence of large spanwise rollers. When permeable substrates are considered, the transpiration is wavelength-dependent, and inhibits the formation of large spanwise structures of wavelengths $\lambda_x^+ \approx 250$, thereby reducing the negative impact.

INTRODUCTION

The development of complex surfaces for turbulent drag reduction has been an area of scientific interest in the last decades. Recently, anisotropic permeable coatings have been proposed by Abderrahaman-Elena & Garcia-Mayoral (2015). They argued that their drag reduction ability is governed by the mechanism established by Luchini *et al.* (1991), Luchini (1996) and Jiménez (1994) for surface textures in general. If the overlying spanwise flow induced by quasi-streamwise vortices is hindered more than the streamwise flow, the vortices are 'pushed away' from the notional wall, decreasing the local momentum flux. This effect can be characterised with the concept of slip length, the depth below the original wall where the tangential velocity becomes zero if extrapolated. Luchini (1996) and Jiménez (1994) proposed that drag reduction is proportional to the offset between the streamwise and spanwise slip lengths, $DR = \Delta c_f / c_f \propto \ell_x^+ - \ell_z^+$.

For the case of anisotropic permeable substrates, Abderrahaman-Elena & Garcia-Mayoral (2015) established a relationship between slips lengths and permeabilities, concluding that for these type of surfaces and for $Re_\tau \approx 1000 - 10000$ drag reduction is approximately

$$DR \approx 0.04 \left(\sqrt{K_x^+} - \sqrt{K_z^+} \right), \tag{1}$$

where K_x^+ and K_z^+ are the streamwise and spanwise permeabilities measured in wall units. However, as these permeabilities increase, the linearised theory of Luchini (1996) and Jiménez (1994) cease to hold as additional, degrading mechanisms set on. For riblets, the degradation is caused by the appearance of elongated, spanwise coherent rollers that arise from a Kelvin-Helmholtz instability (García-Mayoral & Jiménez, 2011). These drag-degrading Kelvin-Helmholtz rollers have also been reported over permeable substrates (Breugem *et al.*, 2006; Kuwata & Suga, 2016). More specifically, Jiménez *et al.* (2001) reported the presence of such rollers over walls permeable in the wall normal direction alone.

Based on the above evidence, Abderrahaman-Elena & Garcia-Mayoral (2015) discussed how the performance of drag reducing permeable coatings would be limited by the triggering of Kelvin-Helmholtz rollers for sufficiently large permeabilities. This phenomenon could also explain the similarities between the drag reduction curves of riblets and that for seal fur (Itoh *et al.*, 2006), which can be viewed as an anisotropic permeable material. Based on the limiting character of the Kelvin-Helmholtz instabilities, guidelines for optimal configurations can be obtained, as well as rough estimates to bound the maximum drag reduction achievable.

The flow within the substrate can be modelled as a continuum using for instance volume-averaged Navier-Stokes (VANS) (Rosti *et al.*, 2015), homogenisation (Zampogna & Bottaro, 2016; Lacis & Bagheri, 2017) or Darcy-Brinkman's equation (Abderrahaman-Elena & Garcia-Mayoral, 2015). Here, the latter approach is chosen, since it allows for an analytical solution. Note however the limitations of this approach, as it implies that the pores are vanishingly small compared to the near-wall turbulent structures, and, in fact, to any lengthscale relevant in the flow.

In their previous work, Abderrahaman-Elena & Garcia-Mayoral (2015) proposed an inviscid linear stability analysis to capture the appearance of Kelvin-Helmholtz rollers, since Kelvin-Helmholtz is an inviscid instability. This implied that the flow could slip freely over the substrate, and no shear could be transmitted to the flow within. Therefore, they neglected the diffusive Brinkman term from the equation describing the underlying flow, as it is typically important only in boundary regions to satisfy no-slip conditions.

In the present project we revisit the above analysis to study the effect of the Brinkman term within the permeable substrate, and the viscous terms on the external channel flow. We subsequently undertake DNSs to gain more detailed insight on the overlying flow. We study channels of height 2δ delimited by two identical anisotropic permeable layers, characterised by their thickness h and their permeabilities in the streamwise x, wall-normal y, and spanwise z directions, K_x, K_y and K_z respectively. We assume these to be the principal directions of the permeability tensor $\mathbf{K}$.

FLOW WITHIN THE PERMEABLE SUBSTRATE

The effect of a permeable substrate on the overlying flow can be represented by slip and impedance boundary conditions at the interface (Jiménez *et al.*, 2001; Hahn *et al.*, 2002; Abderrahaman-Elena & Garcia-Mayoral, 2015). Here we solve the flow within the permeable coating analytically to obtain the boundary conditions that will be later implemented in the linear stability analysis and DNS of the channel.

We model the flow within the substrate through the Darcy-

Brinkman equations,

$$\nabla p = -\nu \mathbf{K}^{-1}\mathbf{u} + \nu\nabla^2\mathbf{u}. \tag{2}$$

where ν is the viscosity. The Brinkman term $\nu\nabla^2\mathbf{u}$ accounts for diffusion effects on scales larger than those integrated through volume averaging into Darcy's term, and allows for continuity of both the velocity and the shear stress at the boundaries. The problem can be expanded in Fourier series in x and z, and its analytical solution provides the following relationships between the velocities and the pressure at the substrate-channel interface,

$$\hat{v}|_{y=0^+} = \hat{v}|_{y=0^-} \equiv \mathscr{C}_{v1}\hat{p}|_{y=0^+} + \mathscr{C}_{v2}\left.\frac{d\hat{u}}{dy}\right|_{y=0^+} + \mathscr{C}_{v3}\left.\frac{d\hat{w}}{dy}\right|_{y=0^+}, \tag{3a}$$

$$\hat{u}|_{y=0^+} = \hat{u}|_{y=0^-} \equiv \mathscr{C}_{u1}\hat{p}|_{y=0^+} + \mathscr{C}_{u2}\left.\frac{d\hat{u}}{dy}\right|_{y=0^+} + \mathscr{C}_{u3}\left.\frac{d\hat{w}}{dy}\right|_{y=0^+}, \tag{3b}$$

$$\hat{w}|_{y=0^+} = \hat{w}|_{y=0^-} \equiv \mathscr{C}_{w1}\hat{p}|_{y=0^+} + \mathscr{C}_{w2}\left.\frac{d\hat{u}}{dy}\right|_{y=0^+} + \mathscr{C}_{w3}\left.\frac{d\hat{w}}{dy}\right|_{y=0^+}, \tag{3c}$$

where the hat indicates variables in Fourier space. The constants $\mathscr{C}_i$ depend on the geometry of the permeable coating through K_x, K_y, K_z and h, but also on the streamwise and spanwise wavenumber. The corresponding expressions can be obtained for the upper wall by symmetry, and together they provide boundary conditions for the flow within the channel.

LINEAR STABILITY ANALYSIS

As mentioned before, the appearance of drag-degrading Kelvin Helmholtz rollers has already been reported over permeable walls (Jiménez *et al.*, 2001; Breugem *et al.*, 2006; Kuwata & Suga, 2016). Therefore, in order to bound the range of optimum parameters which will be investigated later in the DNS simulations, we aim to predict the formation of these spanwise coherent rollers.

Following Jiménez *et al.* (2001), García-Mayoral & Jiménez (2011) and Abderrahaman-Elena & Garcia-Mayoral (2015), a linear stability analysis is performed to capture the formation of Kelvin-Helmholtz rollers. From Squire's theorem we anticipate that oblique modes are more stable than the corresponding two-dimensional ones, which is in agreement with Kelvin-Helmholtz rollers being predominantly spanwise-coherent, so we focus on spanwise-homogeneous modes and perform a two-dimensional, viscous analysis.

Linearising Navier-Stokes' equations about an approximate mean turbulent profile derived by Cess (1958) and considering normal-mode solutions of the form $v' = \hat{v}(y)\exp(i(\alpha x - \omega t))$, Orr-Sommerfeld's equations are obtained,

$$\left[(\alpha U - \omega)\left(D^2 - \alpha^2\right) - \alpha\frac{d^2U}{dy^2} + i\nu_T(D^2-\alpha^2)^2 + i2\frac{d\nu_T}{dy}\left(D^3 - \alpha^2 D\right) + i\frac{d^2\nu_T}{dy^2}\left(D^2+\alpha^2\right)\right]\hat{v} = 0. \tag{4}$$

At the boundaries, we impose continuity of the wall-normal velocity and the pressure as in Abderrahaman-Elena & Garcia-Mayoral (2015), plus continuity for the shear stress and streamwise velocity, which were not required in the inviscid analysis.

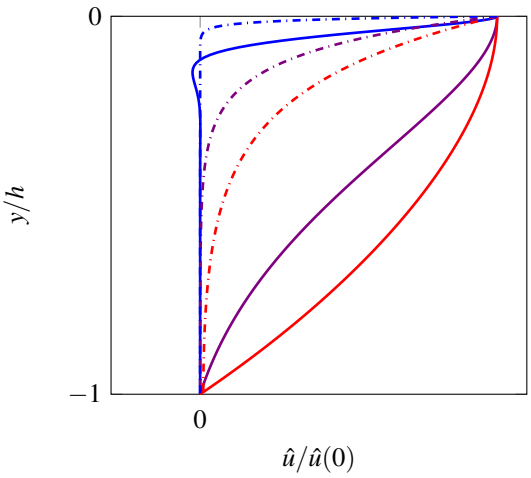

Figure 1: Streamwise velocity profiles within the permeable substrate for $K_x^+ = 100$ and $K_y^+ = 1$, and three different thicknesses: $h^+ =$ (red) 5, 10, (blue) 100. ——, Brinkman's solution; – –, Darcy's solution.

The corresponding boundary conditions are derived from the flow within the permeable substrate. Taking the lower channel wall, $y = 0$, the boundary conditions are given by Eq. (3a) and (3b), with $\mathscr{C}_{u_3} = \mathscr{C}_{v_3} = 0$. The consideration of viscous effects modifies the problem qualitatively compared to Abderrahaman-Elena & Garcia-Mayoral (2015). In the previous work, the problem reduced to Rayleigh's equation with boundary conditions of the form $\hat{v}|_{y=0^+} = \hat{v}|_{y=0^-} \equiv \mathscr{C}_{Darcy}\hat{p}|_{y=0^+}$, while the tangential velocity could slip freely.

Results and discussion

The main difference between the new analysis and that carried out by Abderrahaman-Elena & Garcia-Mayoral (2015) results from the characterisation of the flow within the permeable substrate. To illustrate this, Figure 1 portrays streamwise velocity profiles with and without Darcy's diffusive term, for substrates for which the solutions are particularly different. To emphasize the difference, values have been normalised with the maximum velocity at the interface. Darcy's solution shows a large curvature, differing from the constant velocity profile typical of flows where Darcy's equation is applicable. This discrepancy is due to the large variation of the streamwise pressure gradient $\mathrm{d}p/\mathrm{d}x$ in the wall-normal direction, which is associated to K_y^+. Due to the wall-normal permeability, the pressure decays as it penetrates the coating, so its streamwise pressure gradient is weaker and drives less streamwise velocity, resulting in decaying $\hat{u}$-profile, as shown in Figure 1. The effect is intensified for low wall normal permeabilities, which are actually more efficient for drag reduction, and the Brinkman term $\nu\nabla^2\mathbf{u}$ evaluated from these solutions would be non-negligible.

From the stability analysis, we observe two qualitatively different behaviours for $K_x > K_y$ and $K_x < K_y$. Here results for the case of practical application for drag reduction, $K_x > K_y$, are reported. Results for $K_x < K_y$ can be found in Sharma *et al.* (2016) and are qualitatively similar to those on Abderrahaman-Elena & Garcia-Mayoral (2015). Fig. 2a shows the results from the stability analysis, where the growth rate ω_i^+ is portrayed as a function of the streamwise wavelength λ^+ for different substrate configurations. The asymptotic value of the wavelength at which the maximum growth rate takes place corresponds to the wavelength of Kelvin-Helmholtz rollers. This peak is reached at $\lambda^+ \approx 70$, which is slightly shifted from $\lambda^+ \approx 60$ compared to the inviscid analysis, probably due to the stronger effect of viscosity on smaller wave-

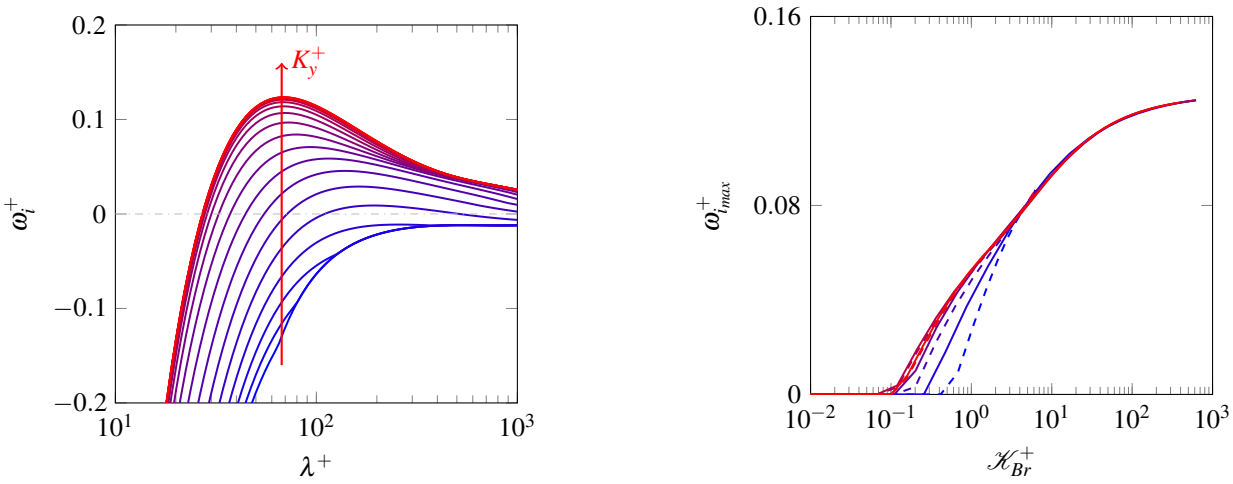

(a) (b)

Figure 2: (a) Growth rate as a function of λ^+ for $h^+ = 100$ and $K_x^+ = 100$. (b) Maximum growth rate $\omega_{i_{max}}^+$ as a function of $\mathscr{K}_{Br}^+$ for different coatings. ——, $h^+ = 100$; – –, $h^+ = 10$. $K_x/K_y =$ (blue) 0, 10, 100, (red) 1000

lengths. The similarity was indeed predictable, since the instability is essentially inviscid, and its wavelength is essentially set by the shape of the mean velocity profile alone. The reason is that $\mathrm{d}^2U/\mathrm{d}y^2$ is the driving term in the Orr-Sommerfeld equation, and near-wall turbulent profiles experience a concentration of $\mathrm{d}^2U/\mathrm{d}y^2$ at $y_c^+ \simeq 9$ independently of the Reynolds number (García-Mayoral & Jiménez, 2011).

In what follows we focus on the most unstable mode, as it is the dominant one. To characterise permeable substrates easily, following Abderrahaman-Elena & Garcia-Mayoral (2015) we propose a single, empirically fitted parameter to define the amplification of the most unstable mode,

$$\mathscr{K}_{Br}^+ = K_y^+ \tanh\frac{\sqrt{2K_x^+}}{y_c^+}\tanh^2\frac{h^+}{4\sqrt{K_y^+}}, \qquad (5)$$

Different coatings with the same value of $\mathscr{K}_{Br}^+$ exhibit essentially the same stability properties. Fig. 2b portrays the amplification of the most unstable mode for a wide variety of coatings with different geometrical parameters K_x, K_y and h, and shows that the effect of these parameters scales in viscous units and is essentially captured by $\mathscr{K}_{Br}^+$. In this Figure two different regions can be distinguished, a low-$\mathscr{K}_{Br}^+$ region, where the Kelvin-Helmholtz modes are not amplified, and a large-$\mathscr{K}_{Br}^+$ region –the asymptotic region–, where Kelvin-Helmholtz rollers are fully developed. We can then define an intermediate region for the onset of the rollers. For sufficiently deep coatings, the hyperbolic tangent terms are ≈ 1, and h^+ and K_x^+ have little effect on the onset of the instabilities. The driving parameter becomes then essentially $\mathscr{K}_{Br}^+ \approx K_y^+$. We note that this is a better estimate than that obtained by Abderrahaman-Elena & Garcia-Mayoral (2015) neglecting diffusive effects in the substrate, $\sqrt{K_x^+K_y^+}$. From Fig. 2b it can be inferred that the triggering of the instabilities occurs for $\mathscr{K}_{Br}^+\big|_{lim} \approx K_y^+ \approx 1-5$. Beyond this threshold the Kelvin-Helmholtz rollers would be fully developed, degrading the drag as in García-Mayoral & Jiménez (2011).

As the wall-normal permeability is essentially the determining parameter, the flow within the permeable substrate can be scaled using K_y^+. Figure 1 suggests that the velocity profile within the coating is self similar, provided that the coating is sufficiently deep for the top-surface-driven flow to decay before reaching the bottom of the

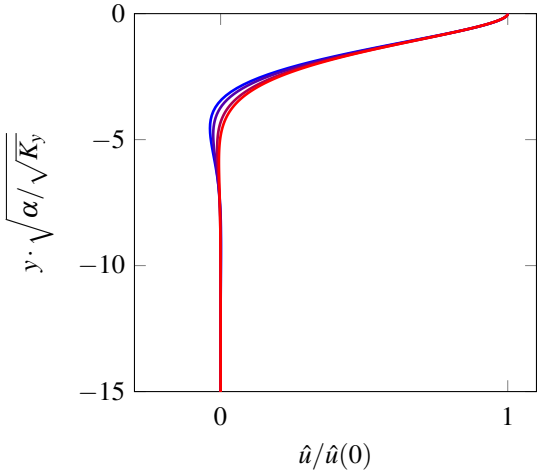

Figure 3: Self-similar streamwise velocity profiles within the permeable substrate for different coatings.

substrate. Self similarity implies that the flow can be characterised by the velocity at the interface, and the penetration depth, which is found to be $\sqrt{\alpha/\sqrt{K_y}}$. The self-similarity of the velocity profiles can be seen in Figure 3.

An order of magnitude analysis shows that, in the free flow channel region, viscous terms are negligible compared to the advective ones, even when the diffusive terms in the permeable substrate must be retained. We have therefore conducted an inviscid analysis as in Abderrahaman-Elena & Garcia-Mayoral (2015). The results, not shown, are broadly similar, and differences are only significant for short wavelengths, which are damped more efficiently by viscosity. We can therefore conclude that the inviscid analysis captures the mechanism involved adequately. However, it is crucial to retain Brinkman's diffusive term within the coating. Tests on Eq. (3) indicate that $\mathscr{C}_{v_2}$, $\mathscr{C}_{u_1}$ and $\mathscr{C}_{u_2}$ do not significantly affect the formation of rollers, and that $\mathscr{C}_{v_1}$ is the dominant coefficient. Nevertheless, it should be noted that the values of $\mathscr{C}_{v1}$ are different from those of the impedance coefficient in Abderrahaman-Elena & Garcia-Mayoral (2015).

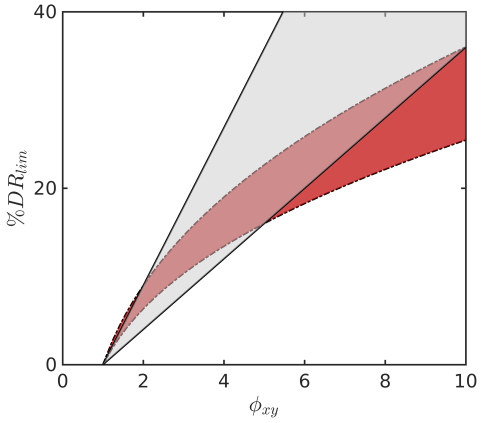

Figure 4: Upper bound for the achievable drag reduction. The red region represents the limit set by modelling the flow in the substrate with Darcy's equations (Abderrahaman-Elena & Garcia-Mayoral, 2015), and the grey region that with Brinkman's. The lower and upper bounds for the regions correspond to $\mathscr{K}^+_{Darcy} = 5$ and 10, and $\mathscr{K}^+_{Br} = 1$ and 5, respectivelly.

Estimating the maximum drag reduction

Let us consider now an anisotropic permeable medium with a preferential permeability in x, and equal permeabilities in y and z, $K_x^+ > K_z^+ = K_y^+$. In the absence of earlier degrading phenomena, we can estimate a tentative threshold for the maximum drag reduction, assuming that up to the Kelvin-Helmholtz limit the linear performance of Eq. 1 holds. Substituting $\mathscr{K}^+_{Br}|_{lim}$ for K_y^+ in Eq. 1 gives

$$DR_{lim} \leq 0.04\sqrt{\mathscr{K}^+_{Br}|_{lim}}\left(\phi_{xy}-1\right), \tag{6}$$

which, once $\mathscr{K}^+_{Br}|_{lim}$ is estimated, is a function of the anisotropy ratio $\phi_{xy} = \sqrt{K_x^+/K_y^+}$ alone, as depicted in Figure 4. We find that the anisotropy effect is stronger than predicted by Abderrahaman-Elena & Garcia-Mayoral (2015), and for large anisotropy ratios the current model produces less conservative bounds for DR_{lim}. These results are encouraging enough to justify a campaign of DNSs to investigate the interaction of the substrate with the near-wall flow.

PRELIMINARY DNS

The DNS code is modified from García-Mayoral & Jiménez (2011). To solve the incompressible Navier-Stokes equations, a fractional step method combined with a three-step Runge-Kutta method is used (Le & Moin, 1991). The spatial discretisation is spectral in x and z using Fourier series, and the wall-normal direction is discretised using a second-order centred finite difference scheme.The simulations are conducted at constant flow rate, starting from a smooth-wall flow at $Re_{\tau_0} \simeq 180$. The computational domain size is $2\pi \times \pi \times 2$ in the streamwise, spanwise and wall-normal directions respectively. A grid with $128 \times 128 \times 153$ points is used, which corresponds to a resolution of $\Delta x_0^+ \approx 8$, $\Delta z_0^+ \approx 4$ and $\Delta y_0^+ \simeq 0.3 - 3$.

Simulations are conducted for a constant mass flow rate in order to validate the results with those obtained by Min & Kim (2004) and Jiménez *et al.* (2001). The change in drag is given by the resulting change in the mean pressure gradient $\mathrm{d}\bar{p}/\mathrm{d}x$,

$$\Delta D = -DR = \frac{\left(-\dfrac{\mathrm{d}\bar{p}}{\mathrm{d}x}\right) - \left(-\dfrac{\mathrm{d}\bar{p}}{\mathrm{d}x}\bigg|_0\right)}{\left(-\dfrac{\mathrm{d}\bar{p}}{\mathrm{d}x}\bigg|_0\right)}. \tag{7}$$

where the subindex 0 denotes the values for a smooth channel, with impermeability and no-slip conditions.

The boundary conditions given by Eq. (3) are used to account for the permeable substrates. In order to understand how these boundary conditions affect the near-wall flow, we preliminarily consider three different cases: (a) MK, with homogeneous streamwise and spanwise slip similar to Min & Kim (2004), (b) MK+J, adding a homogeneous transpiration velocity similar to Jiménez *et al.* (2001) to the previous case; and (c) ES (Equivalent Substrate), with wavelength-dependent transpiration and slip lengths given by Eq. (3). The depth and permeabilities of this substrate were selected to match the slip lengths of MK for homogeneous shear, in accordance with the linearised theory for drag reduction, and to match $\mathscr{C}^+_{v1}$ with the impedance coefficient of MK+J for the lengthscales for which the onset of Kelvin-Helmholtz rollers had previously been observed in DNS (García-Mayoral & Jiménez, 2011), $\lambda_x^+ \approx 150$. The values of the numerical parameters are summarised in table 1.

Case	$\mathscr{C}^+_{v1}$	$\mathscr{C}^+_{u2}$	$\mathscr{C}^+_{w3}$	Re_τ	$\Delta D\%$
MK	-	3.3	3.3	165	-17
MK+J	12	3.5	3.5	184	+5
ES	$K_y^+ = 1$	$K_x^+ = 13$	$K_z^+ = 13$	168	-14

Table 1: Values of the transpiration ($\mathscr{C}^+_{v1}$) and slip lengths ($\mathscr{C}^+_{u2}$ and $\mathscr{C}^+_{w3}$) for the boundary conditions, Re_τ and change in drag compared to the smooth channel of $Re_\tau \simeq 180$.

In these preliminary simulations, only the three coefficients from Eq. (3) which are assumed to drive the modifications in the flow physics have been implemented: $\mathscr{C}_{v1}$, which relates the wall-normal velocity to the pressure fluctuations, as in Jiménez *et al.* (2001), and $\mathscr{C}_{u2}$ and $\mathscr{C}_{w3}$, which represent the slip lengths in the streamwise and spanwise directions, respectively, as in Min & Kim (2004) and Busse & Sandham (2012).

As shown in Figure 5a, the mean streamwise velocity for MK normalised in viscous units agrees with Min & Kim (2004). The velocity profile for the smooth channel has also been included for reference. The upward shift of the logarithmic region with respect to the smooth channel corresponds to a decrease in drag, $DR \simeq 17\%$, which is also in agreement with Min & Kim (2004).

Note that a net drag reduction is obtained in spite of both slip lengths being equal. This is due to a saturation in the spanwise slip beyond $\ell_z^+ \simeq 4$, which is beyond the scope of the present work but was thoroughly examined by Busse & Sandham (2012). On the other hand, when allowing a wall-normal transpiration similar to that of Jiménez *et al.* (2001), a slight increase in drag is observed, as the drag decreasing effect of the slip lengths is outweighted by the drag increasing effect of the wall-normal permeability.

A more realistic way of characterising the permeable substrate is using wavelength-dependent coefficients, as in case ES, for which

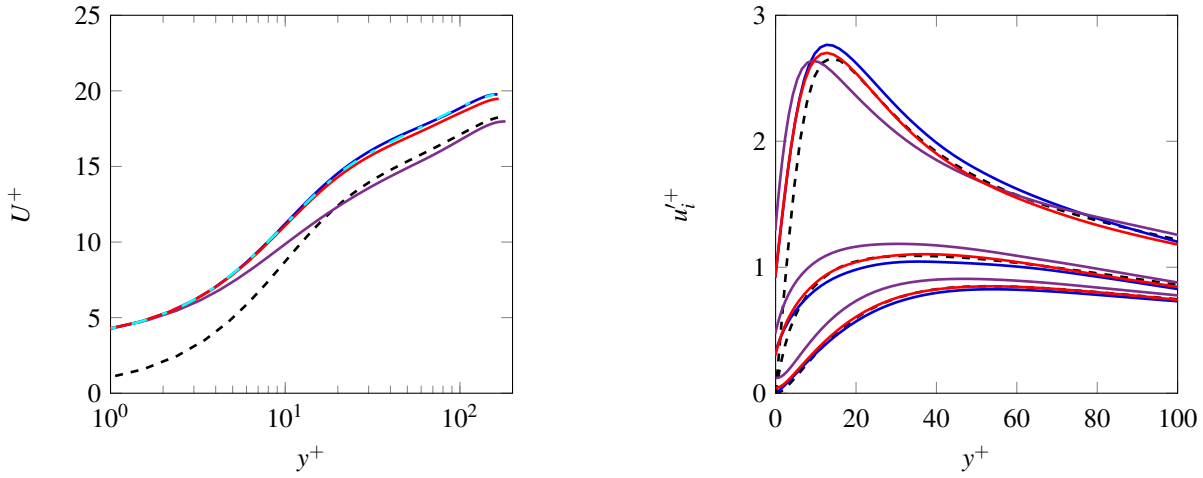

(a) (b)

Figure 5: (a) Mean velocity profiles and (b) rms velocity fluctuations, normalised by their friction velocity. Dashed, smooth channel; dashed-dotted light blue, data from Min & Kim (2004); dark blue, case MK; purple, case MK+J; red, case ES.

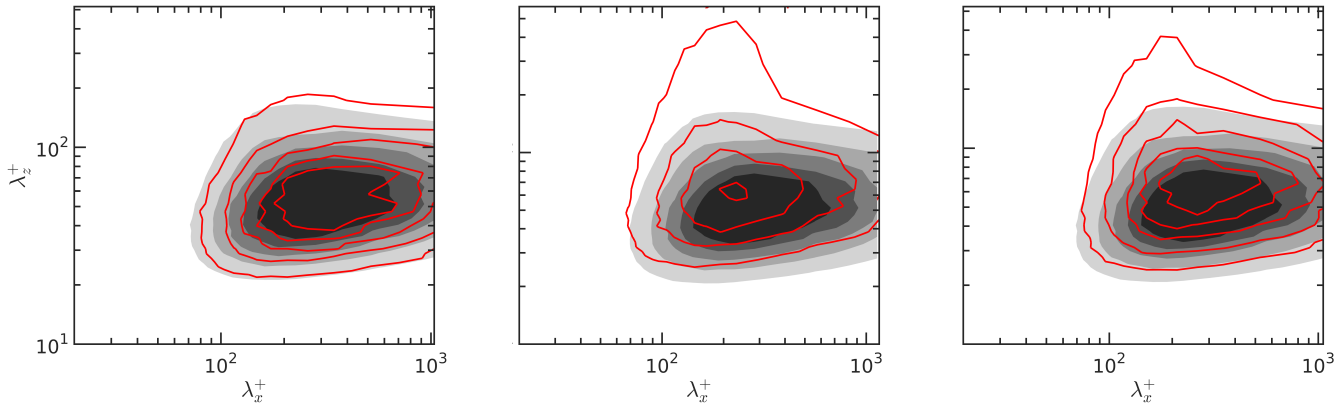

(a) (b) (c)

Figure 6: Premultiplied spectral density of the wall-normal velocity, $k_x k_z E_{vv}$ at $y^+ = 3$. Shaded, smooth channel; lines, present DNSs. (a) MK, (b) MK+J and (c) ES.

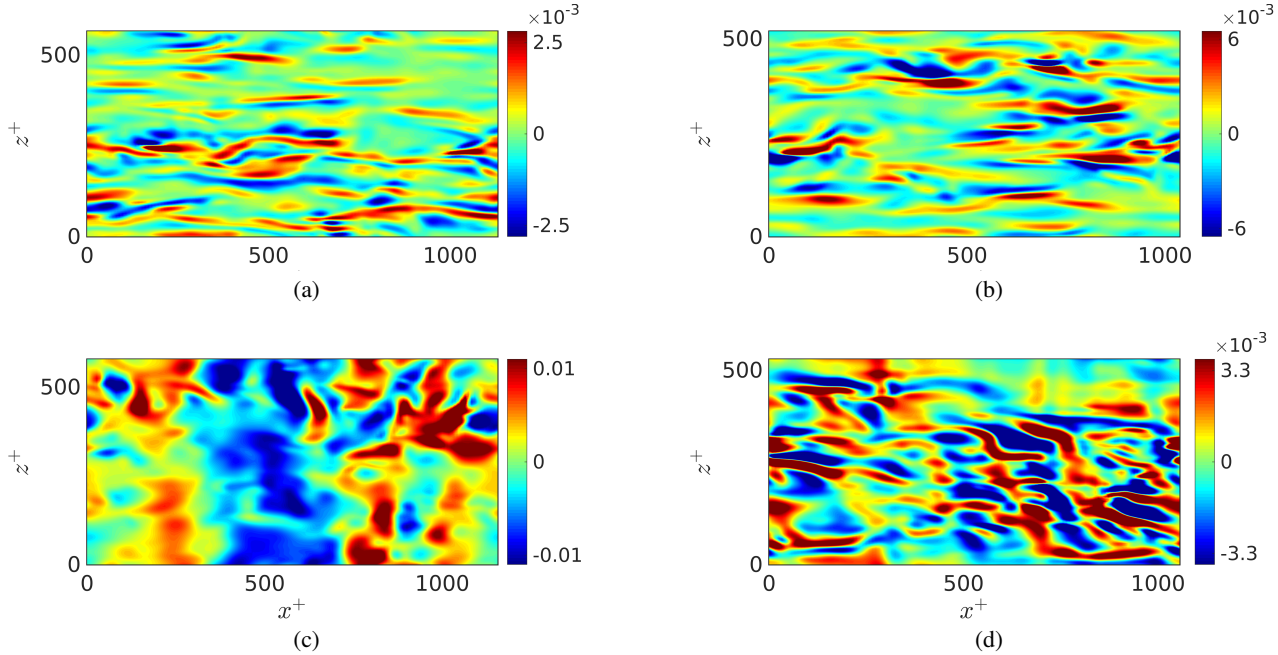

(c) (d)

Figure 7: Instantaneous realisations of wall-normal velocity. (a) Smooth channel at $y^+ = 2$. (b) MK at $y^+ = 2$. (c) MK+J at $y^+ = 0$. (d) ES at $y^+ = 0$.

the slip and transpiration is different at different lengthscales. This case corresponds to a permeable substrate of $K_x^+ = K_z^+ \simeq 13$ and $K_y^+ \simeq 1$ and, compared to MK+J, recovers a significant drag decrease. The reason is that $\mathscr{C}_{v1}^+$, which was set to match MK+J for $\lambda_x^+ \simeq 150$, is smaller at larger wavelengths, inhibiting the formation of the larger-scale rollers observed in MK+J and Jiménez *et al.* (2001).

Figure 5a shows the rms velocity fluctuations normalised by their corresponding friction velocity. Results for a smooth channel are also shown for comparison. As illustrated in the figure, the peak rms values of the streamwise velocity are increased for MK and ES, whereas it is decreased for MK+J. These variations on the fluctuations suggest a modification of the near wall structures.

To gain further insight on the contribution to the rms of different lengthscales, a two-dimensional energy density spectrum of the vertical velocity near the wall is depicted in Figure 6 for our different simulations. While MK does not show a significant difference compared to the case of a smooth channel, for MK+J there is an accumulation of energy at $\lambda_x^+ \approx 250$ and large λ_z^+. Although not shown here, this new energetic region decays at heights above $y^+ \approx 25$. For case ES, on the other hand, the energetic peak is slightly attenuated and displaced to lower wavelengths, $\lambda_x^+ \approx 150$, similar to those observed over riblets by García-Mayoral & Jiménez (2011).

The presence of these energetic structures can also be shown in the instantaneous realisations of the wall-normal velocity depicted in Figure 7. For MK+J there are elongated spanwise coherent structures separated by $\lambda_x^+ \approx 250$. Although not shown here, the strength and coherence of the streaky structures is disrupted by these rollers, contributing to a drag degradation, as reported by Jiménez *et al.* (2001) and García-Mayoral & Jiménez (2011). For case ES, however, the large spanwise coherent rollers are inhibited, and smaller spanwise structures appear instead. Although they are still detrimental for drag reduction, their impact is smaller than in case MK+J.

CONCLUSIONS AND FURTHER WORK

Following previous work, we have considered anisotropic permeable coatings for turbulent drag reduction, focusing on the development of drag-degrading, Kelvin-Helmholtz instabilities over them. We have conducted a new stability analysis on the mean flow above the permeable substrate, taking into consideration large-scale diffusive effects within the coating and viscous effects in the overlying flow. The resulting problem requires additional boundary conditions for the tangential velocity at the interface, which was previously free to slip. It is shown in this more refined analysis that the wall-normal permeability K_y^+ is the governing parameter for the triggering of Kelvin-Helmholtz rollers. Furthermore, the effect of anisotropy is stronger than previously predicted, and higher estimates for the maximum achievable drag reduction can be obtained.

Nevertheless, the instabilities considered may be preceded by other degrading phenomena, which are not predicted in the present theoretical framework. Using the present analysis as a guideline for coating configurations, we are currently undertaking DNSs of channels with permeable substrates. Preliminary DNSs show the formation of drag-degrading spanwise coherent structures due to the relaxation of wall-normal impermeability. However, when realistic permeable substrates are considered, for which the transpiration is wavelength-dependent, drag is less degraded than for a homogeneous transpiration. This is found to be because of greater damping of the larger structures, which decreases the turbulent mixing, and hence, the degradation of drag.

REFERENCES

Abderrahaman-Elena, N. & Garcia-Mayoral, R. 2015 Preliminary analysis of turbulent coatings for turbulent drag reduction. In *Proceedings of TSFP9*.

Breugem, W. P., Boersma, B. J. & Uittenbogaard, R. E. 2006 The influence of wall permeability on turbulent channel flow. *J. Fluid Mech.* **562**, 35.

Busse, A. & Sandham, N. 2012 Influence of an anisotropic slip-length boundary condition on turbulent channel flow. *Phys. Fluids* **24**.

Cess, R. D. 1958 A survey of the literature on heat transfer in turbulent tube flow. Report 8-0529-R24. Westinghouse Research.

García-Mayoral, R. & Jiménez, J. 2011 Hydrodynamic stability and breakdown of the viscous regime over riblets. *J. Fluid Mech.* **678**, 317–347.

Hahn, S., Je, J. & Choi, H. 2002 Direct numerical simulation of turbulent channel flow with permeable walls. *J. Fluid Mech.* **450**, 259–285.

Itoh, M., Tamano, S., Iguchi, R., Yokota, K., Akino, N., Hino, R. & Kubo, S. 2006 Turbulent drag reduction by the seal fur surface. *Phys. Fluids* **18** (6).

Jiménez, J. 1994 On the structure and control of near wall turbulence **944**.

Jiménez, J., Uhlmann, M., Pinelli, A. & Kawahara, G. 2001 Turbulent shear flow over active and passive porous surfaces. *J. Fluid Mech.* **442**, 89–117.

Kuwata, Y & Suga, K 2016 Lattice Boltzmann direct numerical simulation of interface turbulence over porous and rough walls. *Int. J. Heat Fluid Flow* **0**, 1–13.

Lacis, U. & Bagheri, S. 2017 A framework for computing effective boundary conditions at the interface between free fluid and a porous medium. *J. Fluid Mech.* **812**, 866–889.

Le, H. & Moin, P. 1991 An improvement of fractional step methods for the incompressible navier-stokes equations. *J. Fluid Mech.* **92**, 369–379.

Luchini, P. 1996 In *Comput. Methods Appl. Sci. Proc. 3rd ECCOMAS CFD Conf*, pp. 466–470.

Luchini, P., Manzo, F. & Pozzi, A. 1991 Resistance of a grooved surface to parallel flow and cross-flow. *J. Fluid Mech* **228**, 87–109.

Min, T. & Kim, J. 2004 Effects of hydrophobic surface on skin-friction drag. *Phys. Fluids* **16**.

Rosti, M., Cortelezzi, L. & Quadrio, M. 2015 Direct numerical simulation of turbulent channel flow over porous walls. *J. Fluid Mech.* **784**, 396– 442.

Sharma, A., Gomez-de Segura, G. & Garcia-Mayoral, R. 2016 Linear stability analysis of turbulent flows over dense filament canopies. In *Proceedings of TSFP10*.

Zampogna, G. A. & Bottaro, A. 2016 Fluid flow over and through a regular bundle of rigid fibres. *J. Fluid Mech.* **792**, 5–35.